18 MAY 2002, ASTRO-PH/0205333 (ELECTRONIC PREPRINT ONLY)
Preprint typeset using LaTeX style emulateapj v. 04/03/99

ON THE DISCREPANCY BETWEEN *CHANDRA* AND *XMM* TEMPERATURE PROFILES FOR A1835

MAXIM MARKEVITCH
Harvard-Smithsonian Center for Astrophysics, 60 Garden St., Cambridge, MA 02138; maxim@head-cfa.harvard.edu

18 May 2002, astro-ph/0205333 (electronic preprint only)

ABSTRACT

This short technical note addresses a large discrepancy between the temperature profiles for the galaxy cluster A1835 derived by Schmidt et al. (2001) using *Chandra* and by Majerowicz et al. (2002) using *XMM*. The causes of this discrepancy may be instructive for the *Chandra* and *XMM* cluster analyses in general. The observation used by Schmidt et al. was affected by a mild background flare that could not be identified by the usual technique. This flare biased upwards the measured temperatures at large radii. The remaining discrepancy appears to be due to the *XMM* PSF scattering that was not taken into account in the published analyses. While the *XMM* PSF is narrow, the surface brightness of a typical cluster also declines very steeply with radius. For the moderately distant, cooling flow cluster A1835, about 1/3 of the observed *XMM* brightness *at any radius* is due to the PSF scattering from the smaller radii. As a result, the contamination from the bright cool cluster center biases low the measured temperatures near the core, and in general, any temperature gradients are underestimated.

1. INTRODUCTION

A1835 is a moderately distant ($z = 0.25$), symmetric cluster with a strong central X-ray brightness peak. Using *Chandra* data, Schmidt et al. (2001) measured its temperature profile out to $r = 4'$. It revealed a cool center and a temperature increase to ~ 13 keV at $r = 0.5-1\ h_{50}^{-1}$ Mpc. However, Majerowicz et al. (2002) derived a very different temperature profile from the *XMM* data. While they confirm the presence of the cool central region, their outer temperature reaches only ~ 7 keV. The two profiles in the common range of radii are shown in Fig. 1. Such a discrepancy at the qualitative level merits detailed investigation. I first re-analyze the *Chandra* data.

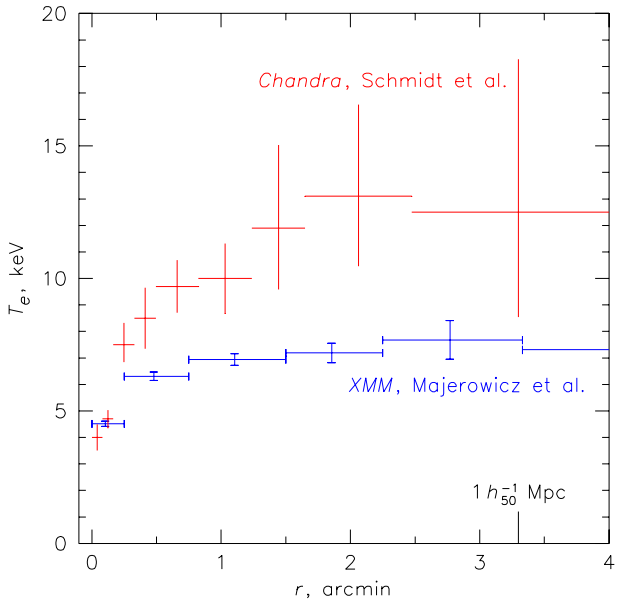

FIG. 1.— Published *Chandra* (Schmidt et al.) and *XMM* (Majerowicz et al.) temperature profiles for A1835. Errors are 90%.

2. *CHANDRA* ANALYSIS

There were 2 *Chandra* observations of A1835, with the cluster in the ACIS S3 chip in both. One (OBSID 495) with a 19 ks exposure was performed on 1999-12-11, and another (OBSID 496) with an 11 ks exposure was done on 2000-04-29. Schmidt et al. used only OBSID 495 for their spectral analysis. They used 0.5–7 keV energy band for spectral fitting and the public blank field dataset for background modeling. In OBSID 495, only one backside-illuminated (BI) chip, S3, was used, and it was almost completely covered by the cluster emission. This presents a difficulty for identifying the background flares (see Markevitch 2001a) using the background light curve. A light curve extracted from a region of the S3 chip far from the cluster center does not vary beyond the normally acceptable $\pm 20\%$ range from the mean (in agreement with the Schmidt et al. conclusions), although due to the cluster contamination, one cannot compare that mean value to the nominal background rate. In OBSID 496, one can also use S1 (another BI chip) for flare detection; neither S1 nor S3 (its part far from the cluster center) show any flares.

Since the quiescent background is known to vary on long and short timescales at a few percent level, for each observation, I calculated the normalizations of the corresponding blank-field datasets from the ratios of count rates in the 10-12 keV band (which is free of the source emission and of the most common variety of flares). As expected, such normalizations were within a few % of the respective exposure ratios.

ARFs and RMFs are calculated as described in, e.g., Markevitch & Vikhlinin (2001). The recently discovered low-energy ACIS quantum efficiency change was corrected; it is not important for the present analysis. N_H was fixed at the Galactic value and abundances at 0.3 solar.

For OBSID 495, using the same background and energy band as Schmidt et al., I obtain a temperature profile very similar to theirs.

2.1. *Soft Galactic background excess*

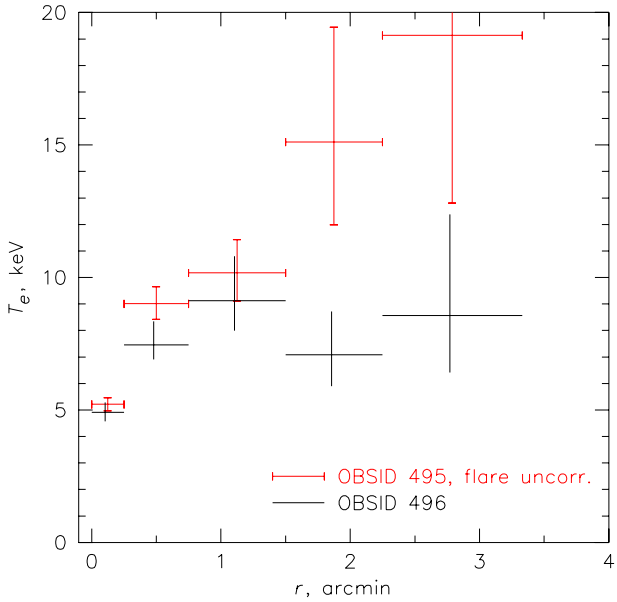

FIG. 2.— *Chandra* A1835 temperature profiles from observations OBSID 495 (the one analyzed by Schmidt et al.) and OBSID 496, derived using the 0.8–8 keV band. The soft Galactic background excess component was accounted for. Errors are 90%.

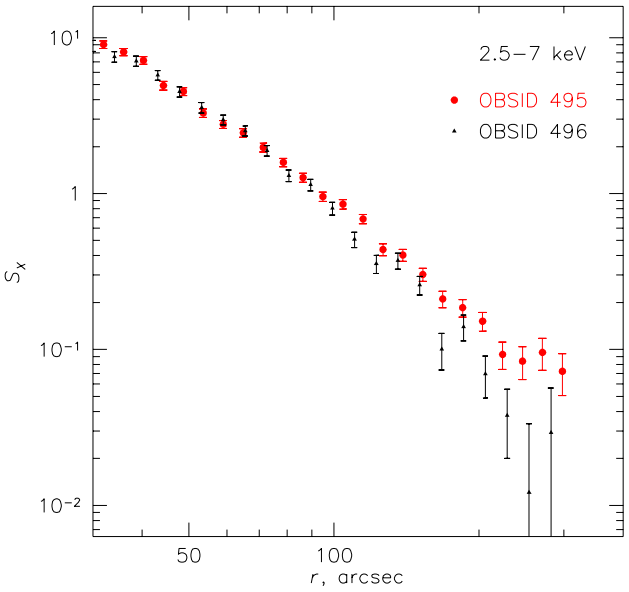

FIG. 3.— *Chandra* radial brightness profiles from OBSIDs 495 and 496 in the 2.5–7 keV band (most sensitive to the background flares). The S_X scale is arbitrary but the observations are normalized by their exposures. Errors are 1σ. There is a clear background excess in OBSID 495.

However, as pointed out by Majerowicz et al., A1835 is projected onto the Galactic North Polar Spur (Snowden et al. 1997) and thus has anomalously high sky background at $E \lesssim 1$ keV. Since the public ACIS background datasets represent the average high Galactic latitude background (see Markevitch 2001b), this anomaly should be taken into account. To evaluate this soft background excess, I extracted spectra from ACIS chips far from the cluster, subtracted the nominal background, and fit the residuals by an arbitrary model (I used low-temperature MEKAL with solar abundances). This best-fit model (renormalized by the ratio of the solid angles) can then be added to the fits in the interesting cluster regions. This properly takes vignetting into account, assuming that the excess component is indeed celestial in origin and does not vary on the ACIS FOV scale. This method was used for *Chandra* analysis by Markevitch & Vikhlinin (2001), and a similar method (without the modeling step) was used for *XMM* by Pratt et al. (2001) and Majerowicz et al.

For this procedure, a region of chips I2 and I3 at $r > 10'$ (3 Mpc) was used for OBSID 495, and the S1 chip was used for OBSID 496. I created subsets of the blank-sky background datasets for the respective time periods ('B' for OBSID 495 and 'C' for OBSID 496) that included exactly the same blank fields for S3 and those other chips (the next release of the public background files will include such subsets). For the 'C' period, such a subset unfortunately is short and dominated by two pointings toward the Galactic Spur. This resulted in *negative* soft excess for OBSID 496, which was fit by a *negative* model. In OBSID 495, there is a real excess above the blank field background.

The best-fit soft excess (or deficit) was included in the cluster fits, and a low energy cutoff of 0.8 keV was adopted to minimize the associated uncertainty. The resulting radial profiles for the two observations are shown in Fig. 2. The two are inconsistent, and OBSID 495 clearly has a problem.

2.2. *Flare background correction*

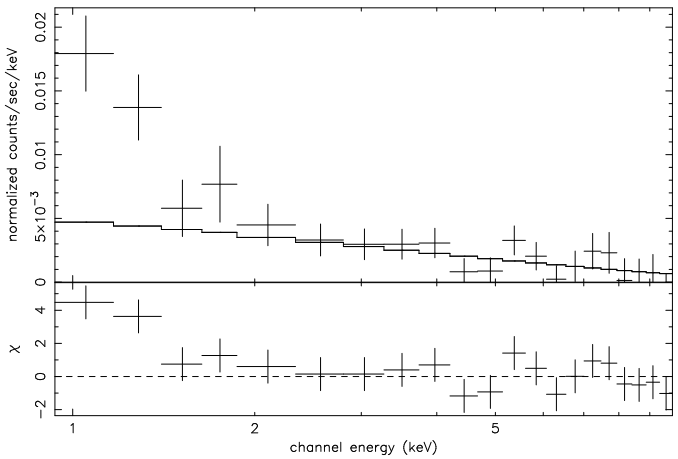

FIG. 4.— Spectrum from the region of the ACIS S3 chip outside $r = 4.5'$ ($1.4h_{50}^{-1}$ Mpc) from the cluster center, with the nominal background subtracted. There is a clear unphysical hard excess, which in the 2.5–7 keV band is consistent with the background flare model (shown by histogram; see text). The residuals at lower energies are due to cluster emission and the Galactic soft background excess.

The most obvious candidate for the problem in OBSID 495 is a mild background flare, which are often observed in the BI chips. It may be too faint or too constant to be identified in the light curve of the relatively short observation (especially if one is using a region containing cluster emission in addition to the background). Spectral shapes of the flare and quiescent background components are such that the 2.5–7 keV band is most sensitive to flares. Fig. 3 shows brightness profiles in this energy band for the two observations, after subtracting the nominal background. OBSID 495 shows a clear background excess.

Figure 4 shows a spectrum of this excess, extracted from the region of the S3 chip outside $r = 270''$ from the cluster center. If the cluster brightness profile from OBSID 496 in Fig. 3 is correct, the true cluster brightness in this band at these large radii is a small fraction of the background excess.

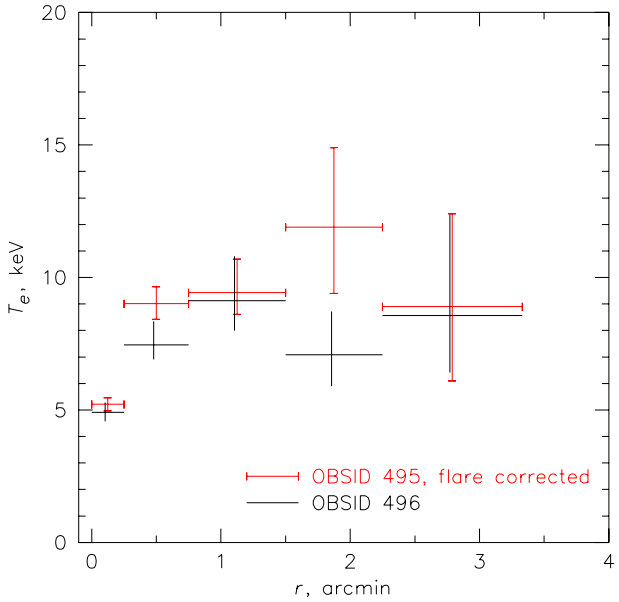

FIG. 5.— *Chandra* profiles from OBSIDs 495 and 496, now with the corrected background flare component in OBSID 495. Errors are 90%.

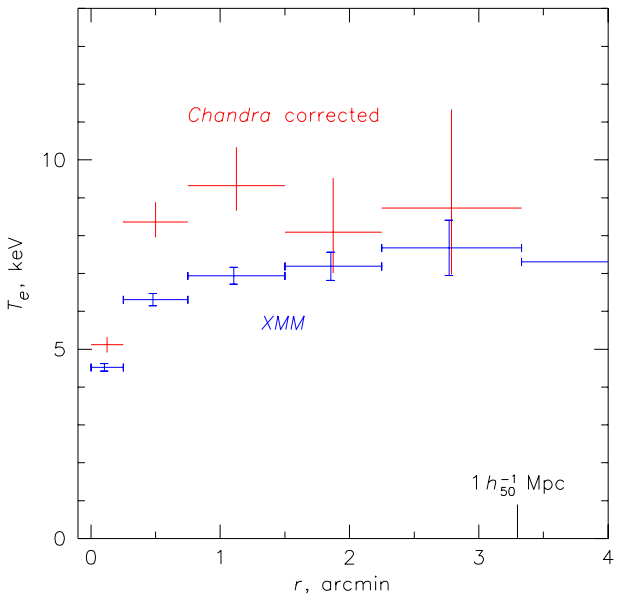

FIG. 6.— The corrected *Chandra* temperature profile (average of 2 observations) and the *XMM* profile. Errors are 90%.

There are at least two species of the background flares observed in the BI chips. The most frequent one affects only the BI chips and is not seen in FI chips. In OBSID 495, there are no flares in the FI chips (this can be established confidently using the regions free of cluster emission covered by those chips). Thus the putative flare in chip S3 should belong to this species. Such flares appear to have the same spectral shape regardless of their brightness, and are well-described by a power law with the photon index $\gamma \approx -0.1$ and an exponential cutoff at $E \approx 5$ keV (Markevitch et al. 2002a) without the application of the telescope or CCD efficiency ('arf none' in XSPEC). Figure 4 shows this model with the normalization fitted to the spectrum in the 2.5–7 keV band. The excess at $E > 2.5$ keV is fully consistent with this model; the residuals at lower energies should be due to the soft Galactic excess (uncorrected for this exercise) and the cluster emission. At $E = 3-5$ keV, the flare brightness is 30–40% of that of the nominal background.

Thus, the hard excess in OBSID 495 is consistent with a mild residual background flare. We can assume (somewhat arbitrarily) that this component is spatially uniform and subtract it from the cluster spectra, normalizing it according to the solid angles. This method was used in Markevitch et al. (2002b). The resulting corrected temperature profile for OBSID 495 is shown in Fig. 5 along with the original profile for the unaffected OBSID 496. A $\pm$40% uncertainty (90% confidence) for the flare component normalization is included in quadrature. The effect of the flare correction is significant at $r > 1'$. After the correction, the two *Chandra* observations become more or less consistent. (Note that the original Schmidt et al. profile shown in Fig. 1 is consistent with the corrected profile; the competing effects of the soft Galactic background excess and the hard flare excess partially compensated for each other in that work.)

Figure 6 overlays the corrected *Chandra* temperature profile on the *XMM* profile; there is still a significant discrepancy.

3. *XMM* PSF EFFECT

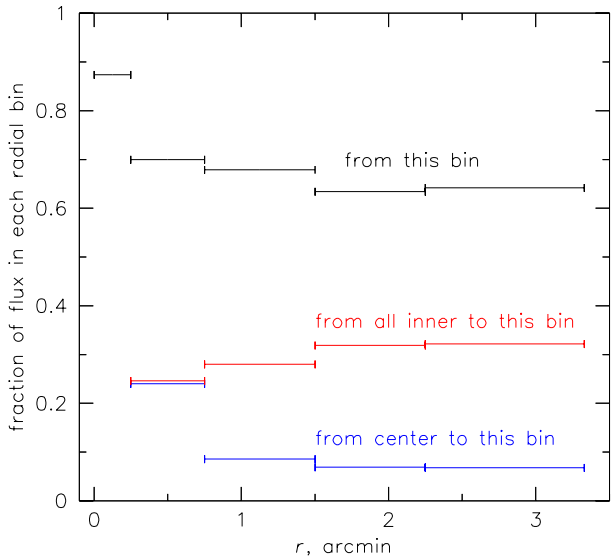

FIG. 7.— Fraction of the observed flux in each *XMM* annulus originating from the same annulus in the sky, and fractions scattered by the telescope from the central circle and from all inner regions including the center.

The obvious candidate for the remaining discrepancy is the *XMM* PSF, which was not included in any currently published *XMM* analyses. For a quick estimate of the PSF effect, I use on-axis MOS1 PSF in the 0.75–2.25 keV band presented in "*XMM-Newton* Users' Handbook".[1] It can be described by the function $S_X \propto (1+r^2/r_c^2)^{-\alpha}$ with $r_c = 3.5''$, $\alpha = 1.36$. Ignoring its dependence on coordinate and energy, one can estimate what fraction of the observed *XMM* flux in each region originates in the same region in the sky and how much is scattered from other regions. I used the *Chandra* image of A1835 as a true brightness model (the *Chandra* PSF can be ignored for the present purpose). The model image was cut into annuli (same as used by Majerowicz et al.), each annulus is convolved with the PSF, and contributions from each annulus in the sky into

[1] http://heasarc.gsfc.nasa.gov/docs/xmm/uhb/xmm_uhb.html, sections "X-ray telescopes", "On-axis PSF"

each annulus in the image were calculated.

The result for the inner 5 annuli (those completely covered by *Chandra*) is shown in Fig. 7. Even though the PSF 90% encircled energy radius is only 45–50″, the cluster brightness profile declines so steeply with radius that in each annulus, there is a $\sim$ 10% or higher contribution from the central peak. Furthermore, every annulus has a $\sim$ 30% contamination from the inner regions, with the obvious effect of smearing any temperature gradients in the cluster.

A simple XSPEC simulation (using EPIC responses and the exposure time, energy band and spectral binning given by Majerowicz et al.) shows that if the temperatures from the *Chandra* profile are mixed in the proportion shown in Fig. 7, one can obtain single-temperature EPIC fits very close to those reported. In particular, for the 2nd annulus, I obtain 6.4–6.8 keV compared to *Chandra*'s 8 keV. For the 3rd annulus, I obtain 7.0–7.7 keV compared to *Chandra*'s 9 keV.

4. LESSONS

1. When ACIS background is critical, one should ensure that the quiescent background rate is consistent with the nominal rate (the one in the background datasets), even if there are no obvious signs of background flares in the background light curve. For ACIS BI chips, the 2.5–7 keV band is best for this purpose because it is sensitive to the most common flare species. The next version of the public background datasets for the BI chips will be filtered using this energy band (instead of the presently used wide band).

2. The *XMM* PSF has to be taken into account for the analysis of clusters with peaked X-ray brightness profiles. (Monique Arnaud communicates that it will be included in their forthcoming reanalysis of the A1835 data.)

Incorrect modeling of the *Chandra* background and disregard of the *XMM* PSF appear to explain most if not all of the discrepancy between the recently published A1835 temperature profiles.

This analysis was supported by NASA contract NAS8-39073 and grant NAG5-9945.

REFERENCES

Majerowicz, S., Neumann, D. M., & Reiprich, T. H. 2002, A&A, submitted (astro-ph/0202347)
Markevitch, M. 2001a, memo "ACIS background", http://cxc.harvard.edu/contrib/maxim/bg
Markevitch, M. 2001b, http://cxc.harvard.edu/contrib/maxim/acisbg/data/README
Markevitch, M., & Vikhlinin, A. 2001, ApJ, 563, 95
Markevitch, M., et al. 2002a, in preparation ("*Chandra* spectra of the soft X-ray diffuse background")
Markevitch, M., et al. 2002b, ApJ, 567, L27
Schmidt, R. W., Allen, S. W., & Fabian, A. C. 2001, MNRAS, 327, 1057
Snowden, S. L., et al. 1997, ApJ, 485, 125